Lipopolysaccharide acutely suppresses right-ventricular strain in rats with pulmonary artery hypertension

Junjie Zhang[1], Yanan Cao[1], Xiaowei Gao[1], Maoen Zhu[1], Zhong Zhang[1], Yue Yang[1], Qulian Guo[1], Yonggang Peng[2] and E. Wang[1]

[1]Department of Anesthesiology, Xiangya Hospital, Central South University, Changsha, Hunan, China; [2]Department of Anesthesiology, Shands Hospital, University of Florida, Gainesville, FL, USA

Abstract

Worsening right ventricular (RV) dysfunction in the presence of pulmonary artery hypertension (PAH) increases morbidity and mortality in this patient population. Transthoracic echocardiography (TTE) is a non-invasive modality to evaluate RV function over time. Using a monocrotaline-induced PAH rat model, we evaluated the effect of acute inflammation on RV function. In this study, both PAH and control rats were injected with *Escherichia coli* lipopolysaccharide (LPS) to induce an acute inflammatory state. We evaluated survival curves, TTE parameters, and inflammatory markers to better understand the mechanism and impact of acute inflammation on RV function in the presence of PAH. The survival curve of the PAH rats dropped sharply within 9 h after LPS treatment. Several echocardiographic parameters including left ventricular (LV) stroke volume, RV tricuspid annular plane systolic excursion, RV longitudinal peak systolic strain, and strain rate decreased significantly in PAH rats before LPS injection and 2 h after LPS injection. The expression of phospholamban (PLB) and tumor necrosis factor-α (TNF-α) significantly increased and the expression of SERCA2a significantly decreased in PAH rats after LPS administration. LPS suppressed the RV longitudinal peak systolic strain and strain rate and cardiac function deteriorated in PAH rats. These effects may be associated with the signal pathway activity of SERCA2a/PLB.

Introduction

Pulmonary arterial hypertension (PAH) is characterized by increased pulmonary vascular resistance (PVR), right ventricular (RV) hypertrophy, RV dysfunction, uncompensated right heart failure, and ultimately, death.[1–3] The RV, in response to an increase in afterload, is an important factor in determining the prognosis of patients with PAH.[4] The patients with PAH often manifest rapid progression to heart failure when suffering with pulmonary infection or puerperal infection, yet the underlying mechanism is unclear. Echocardiography cannot only sufficiently assess RV structure and function but can also suggest the prognosis of PAH.[5] Tissue Doppler image (TDI) strain analysis is a novel method to assess RV function. The value of measuring RV strain to detect changes in RV function has been

described.[5] In the small animal research setting, a non-invasive technology, like the echo-based TDI, has many advantages over an invasive RV conductance catheter in measuring pulmonary hypertension (PH) and RV morphology.[6] This study aimed to investigate the pathogenesis of acute RV function decline exacerbated by inflammation in PAH rats. We hypothesized that acute inflammation superimposed on PAH severely deteriorates RV function and that the potential mechanisms for this deterioration include the

Corresponding author:
E. Wang, Department of Anesthesiology, Xiangya Hospital, Central South University, Changsha, Hunan, China.
Email: ewang324@csu.edu.cn

sarcoplasmic reticulum Ca2+ ATPase 2a (SERCA2a)/phospholamban (PLB) pathway.

Methods

PAH model and lipopolysaccharide injection

The protocol was approval by the Ethics Committee for Animal Research of Xiangya Hospital of Central South University (permit no. 201303311). All experimental methods were in accordance with guidelines for treating lab animals. Male adult Sprague-Dawley rats (Laboratory Animal Center of Central South University, Changsha, China) were randomly divided into a control group and the PAH group. The rats in the PAH group were intraperitoneally injected with 1% monocrotaline (60 mg/kg, Sigma-Aldrich, St. Louis, MO, USA). The control group was injected with the equivalent volume of normal saline. All rats were fed with standard chow and tap water in a temperature- and humidity-controlled room with a light–dark cycle. After four weeks, systolic pulmonary arterial pressure (sPAP) was estimated by echocardiography. The rat with sPAP >60 mmHg was taken into the next experiment as a PAH rat.

Rats in both groups were then intraperitoneally injected with *Escherichia coli* lipopolysaccharide (LPS; serotype O55:B5, 1 mg/kg; Sigma-Aldrich). Survival times were recorded and a survival curves were plotted. Echocardiography data were collected from another group of rats at two time points: baseline immediately before LPS injection and 2 h after LPS injection. Heart and lung tissue was harvested for hematoxylin and eosin (H&E) staining. RV cardiomyocytes were isolated for analysis of SERCA2a, PLB, and tumor necrosis factor (TNF)-α expression by western blotting.

Echocardiography

Images were obtained by the Vivid E7 system (General Electric Vingmed, Horten, Norway). Echocardiography examinations were performed after rats were anesthetized with an intraperitoneal injection of ketamine (50 mg/kg, Renfu Pharmaco, Yichang, China). Left ventricular (LV) function was assessed in the mid-LV papillary short axis view. M-mode echocardiography was performed to obtain LV end-diastolic and end-systolic diameters (Fig. 1A). Stroke volume (SV), heart rate (HR), and cardiac output (CO) were measured and recorded. RV systolic pressure
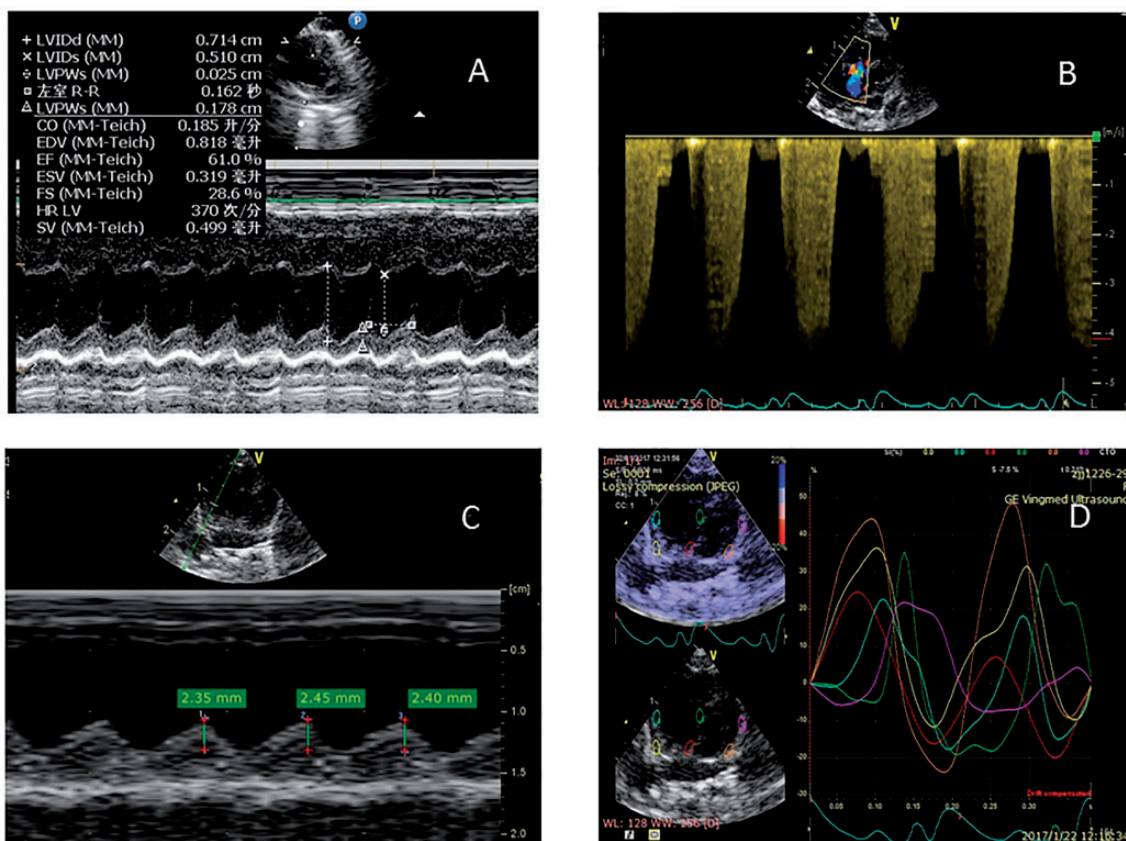

Fig. 1. LV function was measured on the parasternal mid-LV papillary short axis view with M-mode echocardiography (A). PAP was measured by tracing the continuous wave Doppler spectrum of the tricuspid regurgitation jet (B). TAPSE was measured by M-mode Doppler (C). Peak longitudinal systolic strain curve image measured by TVI is shown (D). Strain image curve of regional measurements, i.e. RV free wall basal segment (yellow), mid segment (cyan), septum basal segment (red), and mid segment (green) are shown.

and sPAP were estimated by calculating the maximum velocity of the tricuspid regurgitant jet using the modified Bernoulli equation and an estimated as right atrial pressure of 10 mmHg (Fig. 1B). In an apical four-chamber view using M-mode, the M-mode cursor was positioned on the lateral portion of the tricuspid annulus to measure tricuspid annular plane systolic excursion (TAPSE) (Fig. 1C). RV mid-diameter was measured on the apical four-chamber view. RV stain was derived from the apical four-chamber view using tissue velocity imaging (TVI) with the sample area limited to RV wall. RV longitudinal strain (LS) and longitudinal strain rate (LSR) were determined by TVI (Fig. 1D). The sampled areas were the basal and the mid segment of the free wall. The LS and LSR were recorded before and after LPS administration.

Morphologic study

The surviving PAH rats were anesthetized and euthanized. The lungs were dissected and fixed with 4% paraformaldehyde. The morphological changes in the lung and pulmonary arterial vessels were assessed by H&E staining.

Western blot

The effects of LPS on SERCA2a, phosphorylation PLB (pPLB), and TNF-α expression in RV cardiomyocytes in both groups were analyzed by western blot. The hearts were removed and the RV free walls were dissected from the LV and frozen at −80°C. The proteins of RV cardiomyocytes were extracted and subjected to the western blotting protocol. Total protein extracted from the RV in each group were lysed with RIPA lysis buffer containing a 1:100 dilution of phenylmethanesulfonyl fluoride (Beyotime, Shanghai, China) on ice for 10 min; this was sonicated and centrifuged at 12,000 g for 10 min at 4°C. Protein concentrations were measured with a BCA Protein Assay Kit (Beyotime, Shanghai, China). Equal amounts of the denatured protein (50 μg/lane) were separated by 10% sodium dodecyl sulfate–polyacrylamide gel electrophoresis in a mini-gel apparatus (Mini-PROTEAN II, Bio-Rad, Hercules, CA, USA) and transferred to polyvinylidene fluoride membranes (Merck Millipore, Billerica, MA, USA). After membranes were blocked with 5% bovine serum albumin in Tris-buffered saline plus 0.05% Tween 20 (pH = 7.5) for 1 h, they were incubated overnight at 4°C with primary mouse monoclonal anti-SERCA2 ATPase (1:1000; Abcam, Cambridge, MA, USA), rabbit polyclonal anti-p-PLN (1:1000, Cell Signal Technology, Danvers, MA, USA), rabbit polyclonal anti-TNF-α (1:3000, Merck Millipore), and rabbit monoclonal anti-GAPDH (1:1000, Cell Signal Technology). Membranes were then incubated with a corresponding secondary antibody, horseradish peroxidase-conjugated goat anti-rabbit and anti-mouse antibodies (both 1:4000; ComWin Biotech, Beijing, China), at room temperature for 2 h. Antibodies

were diluted in Tris-buffered saline containing 5% non-fat milk. The bands were visualized using a super enhanced chemiluminescence detection reagent (Merck Millipore). Image Pro Plus 6.0 software was used for densitometry analysis. The results were normalized to GAPDH levels.

Statistical analysis

All data were expressed as the mean ± standard deviation (SD). Paired t-test was used for statistical analysis for the comparison of the groups at baseline and after the LPS treatment. Statistical significance was accepted at $P < 0.05$.

Results

The pulmonary vascular pathological change in PAH rats using H&E staining is shown in Fig. 2. Compared with controls, PAH rats had thicker pulmonary arterial walls and more perivascular inflammatory cellular infiltration. The number of PAH rats that survived with exposure to 1 mg/kg LPS decreased sharply from 12 to zero within 9 h, whereas the same dose of LPS had no effect on the survival of control rats up to 72 h (Fig. 3).

Through echocardiographic measurements (Fig. 1), LV SV, HR, and CO decreased significantly following injection of LPS in the PAH group compared to the control
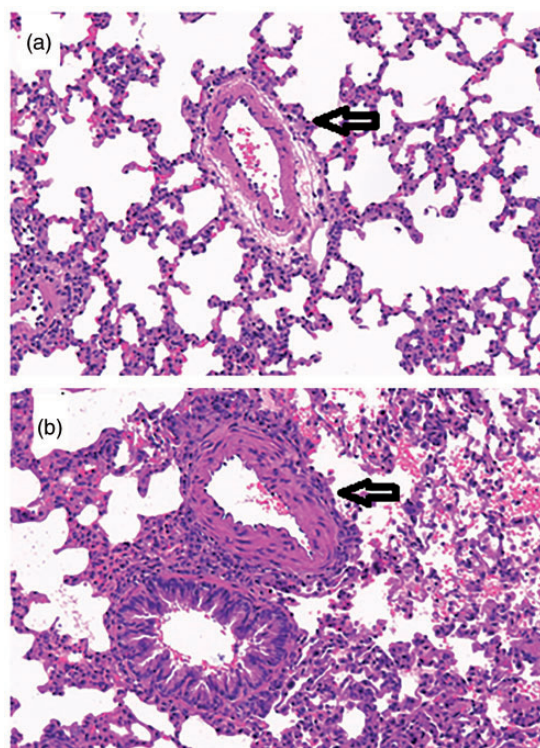

Fig. 2. H&E staining of small pulmonary arteries as pointed arrows is from a control rat (a) and a PAH rat (b). A thickened medial layer and a narrow vessel of a pulmonary arterial vessel are evident in the PAH rat.

group (Table 1). After LPS treatment, the mid-RV diameter increased significantly in both groups, but comparing PAH to controls, this measurement was significantly higher in PAH rats ($P < 0.05$). TAPSE decreased significantly after LPS treatment in both groups as well. The sPAP increased significantly after LPS treatment in the PAH group (Table 1).

Advanced measurements of cardiac performance are represented by RV myocardial regional peak systolic longitudinal strain. Longitudinal strain at the basal and middle segments of RV free wall were reduced following LPS injection in both PAH rats and controls (Table 1). But LPS was significant inhibitor for RV systolic function in PAH rats (Fig. 4).
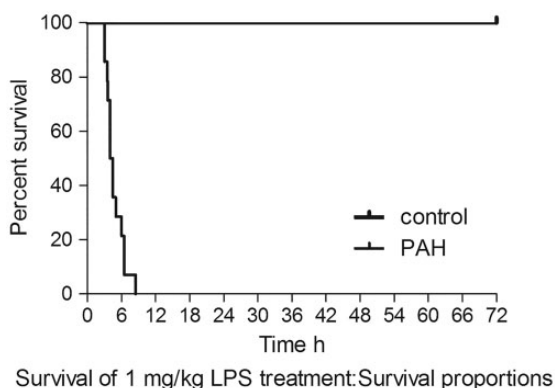

Fig. 3. Representative survival curve of PAH group rats compared with control group rats after non-lethal dose LPS treatment. The survival of PAH rats dropped sharply after LPS administration.

LPS treatment resulted in a significantly increased pPLB protein expression level (Fig. 5a) and decreased SERCA2a protein expression level in myocardial tissue in PAH rats (Fig. 5b). A significantly decreased SERCA2a/pPLB ratio was observed after LPS treatment in PAH rats (Fig. 5c). As expected, LPS also significantly increased TNF-α expression in PAH rats (Fig. 5d).

Discussion

A monocrotaline model is a commonly used animal model that can specifically damage lung vascular endothelial cells, capillaries, and pulmonary arterial walls, leading to pulmonary vascular hyperplasia and vascular and RV remodeling. Gradually increase in PAP can result in RV hypertrophy, while sudden elevation of PVR can lead to decompensated RV failure.[7] In the outpatient setting, stable PH has limited impact on mortality and be compatible with long-term survival. However, in the setting of acute infection or inflammation, PH often progresses to rapid deterioration of cardiac function. The short-term mortality is extremely high in these circumstances. Our PAH rats were injected with LPS to mimic the status of acute inflammation in patients with PAH to explore the mechanism of PAH aggravation. RV failure has no direct relationship with an increasing afterload in this setting, indicating that there is an intrinsic mechanism that drives progression toward RV failure. We speculated that an external environmental factor such as inflammation can be a trigger for the switch from compensated RV hypertension to decompensated RV hypertension. LV end-diastolic volume decreased in PAH rats when compared with controls, possibly as an effect of ventricular interdependence.[8] Although always present,

Table I. Echocardiographic function variables.

Variables	Control group (n = 8)			PAH group (n = 11)		
	Baseline	LPS-treated	P value	Baseline	LPS-treated	P value
LVSV (mL)	0.448 ± 0.142	0.382 ± 0.110	0.069	0.251 ± 0.093	0.175 ± 0.054	0.043
HR (bpm)	424 ± 38	418 ± 13	0.650	390 ± 37	334 ± 55	0.001
CO (L/min)	0.191 ± 0.059	0.164 ± 0.049	0.087	0.101 ± 0.032	0.058 ± 0.020	0.001
RVEDD (mm)	2.960 ± 0.163	3.167 ± 0.195	0.004	4.873 ± 0.287	5.509 ± 0.422	0.000
TAPSE (mm)	3.12 ± 0.24	2.57 ± 0.31	0.001	2.25 ± 0.28	1.58 ± 0.24	0.000
sPAP (mmHg)				74.5 ± 9.1	95.4 ± 13.8	0.001
Strain %						
Basal RV free wall	−19.41 ± 4.77	−15.5 ± 3.21	0.059	−12.18 ± 3.33	−7.54 ± 3.47	0.000
Mid RV free wall	−17.19 ± 4.98	−13.18 ± 2.71	0.057	−11.45 ± 4.74	−7.23 ± 2.94	0.000
Strain rate I/S						
Basal RV free wall	−4.35 ± 1.00	−3.69 ± 1.48	0.331	−4.12 ± 1.32	−2.66 ± 1.12	0.001
Mid RV free wall	−3.97 ± 1.27	−3.20 ± 0.61	0.068	−3.52 ± 1.43	−2.56 ± 1.07	0.014

Values are mean ± SD.
LV SV, LV stroke volume; HR, heart rate; CO, cardiac output; RVEDD, RV end-diastolic diameter; TAPSE, tricuspid annular plane systolic excursion; sPAP, pulmonary artery systolic pressure.
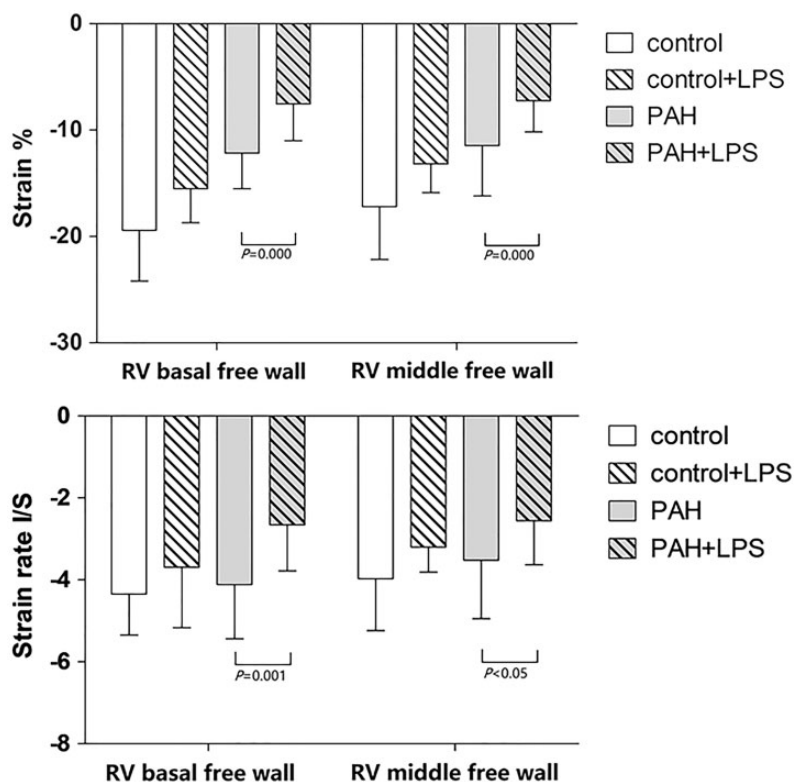
Fig. 4. Strain and stain rate of RV free wall before LPS treatment and 2 h after LPS treatment in both groups of rats. Values are expressed as mean ± SD.
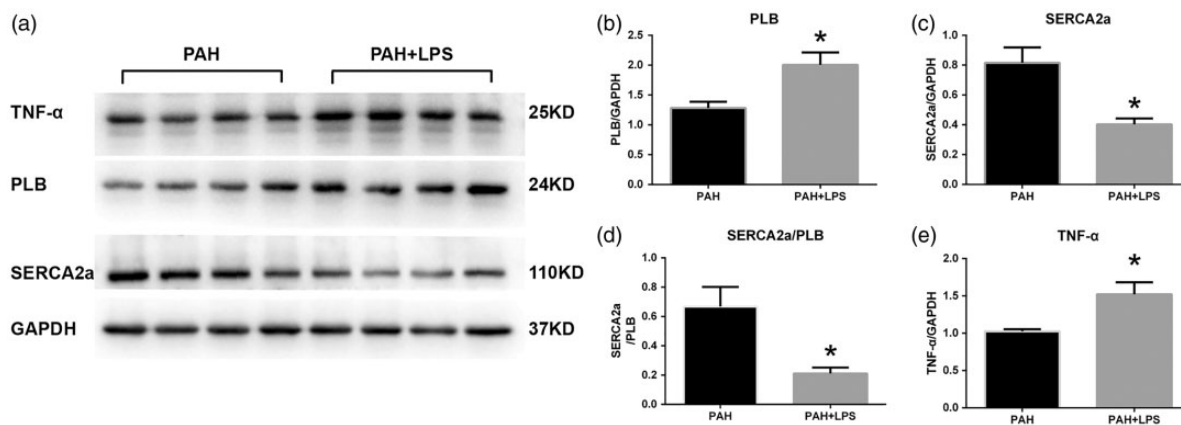

Fig. 5. Changes in phospholamban (PLB; a), SERCA2a (b), the ratio of sarcoplasmic reticulum Ca^{2+} ATPase 2a (SERCA2a)/PLB (c), and tumor necrosis factor (TNF)-α (d) expression in right ventricular myocytes of pulmonary arterial hypertension (PAH) rats after exposure to lipo-polysaccharide (LPS). Representative expression levels of western blots (e). Values are expressed as mean ± SD. *$P < 0.05$.

ventricular interdependence is most apparent with changes in loading conditions.[9] A further reduction of LV function is due to progressive leftward septal displacement.[10] When LPS was administered, LV SV in PAH rats significantly decreased, indicating that acute inflammation exacerbated dysfunction of both RV and LV. We found no significant difference in HR between control rats and PAH rats, but the HR of PAH rats was significantly decreased when LPS was administered. It is reported that LPS has an impaired

frequency-dependent relaxation effect of force-frequency relationships, which shortens LV filling time and decreases stroke volume by 22%. This may be related to an LPS reduction in SERCA-dependent calcium uptake.[11]

TAPSE is an independent prognostic factor for patients with PH and right heart failure.[12–14] In our study, TAPSE decreased significantly in PAH rats, suggesting that RV systolic function was impaired. RV contraction is determined by the anatomy of the myocardium longitudinal stretch;

thus, the evaluation of RV systolic function mainly relies on strain.[4] Impaired longitudinal strain (LS) indicates a poor prognosis for patients with PAH.[15–18] Chu et al. believe that even in mice, the use of strain can detect early LV dysfunction.[19] Our research found that RV strain and strain rate had obviously declined in the presence of acute inflammation in PAH rats. These results reveal why an otherwise nonlethal dose of LPS caused acute RV function failure in PAH rats and led them to die.

It has been reported that RV-pulmonary artery decoupling in right heart failure is associated with downregulation of SERCA2a expression.[20] In the MCT-induced PAH rats, the eNOS, A2AR, SERCA2a, and PLB levels were changed compared with the normal rats and the Ca(2+)-ATPase activity was reduced.[21] The regulation of intracellular free calcium concentration in the normal range is particularly important for myocardial cells, which are regulated mainly by myocardial SERCA2a.[22] A large number of experimental data have shown that PLB mainly regulates uptake and release of calcium by SERCA2a.[23,24] Our group has also demonstrated that rats with chronic, stable PH tolerate low concentrations of sevoflurane inhalation due to modulation of the SERCA2-PLB signaling pathway.[25] In the present study, the expression of SERCA2a was downregulated and phosphorylation PLB was upregulated after LPS treatment in PAH rats. This declined ratio of SERCA2a/pPLB may contribute to ventricular dysfunction. This indicates that the mechanism of RV failure in PAH rats caused by LPS might be mediated by the SERCA/pPLB pathway. It has been found that inducible nitric oxide synthase/soluble guanylate cyclase inflammation signaling pathway modulated RV dysfunction in a rat model of PAH.[26] LPS stimulates the release of TNF-α by inflammatory cells, which in turn leads to various inflammation damage. It is well-known that TNF-α is a manifestation of inflammation and has a negative inotropic effect on cardiomyocytes. It has already been reported that TNF-α expression is elevated in the failing heart and that TNF-α has a negative inotropic effect on cardiomyocytes.[27] In this study, TNF-α was significantly upregulated in PAH rats after LPS administration and in accordance with impairment of cardiac function. Interaction between inflammation and sarcoplasmic reticulum calcium intake needs to be investigated.

An otherwise non-lethal dose of lipopolysaccharide causes rapid deterioration of cardiac function in PAH rats. Despite LPS administration did not resulted in rapid RV failure and mortality in control rats, LPS injection or inflammation process markedly suppressed RV LPSS and strain rate in PAH rats. The effect of LPS on RV function in PAH rats may be associated with SERCA2a/PLB pathway activity.

Limitations

We used the method of tracing the tricuspid regurgitation spectrum to determine PAP. We could not measure PAP if the tricuspid regurgitation was not present. We cannot rule out RV ischemia totally which might contribute to RV failure and death, but through other mechanisms.

Conflict of interest

The author(s) declare that there is no conflict interest.

References

1. Santos-Ribeiro D, Mendes-Ferreira P, Maia-Rocha C, et al. Pulmonary arterial hypertension: Basic knowledge for clinicians. *Arch Cardiovasc Dis* 2016; 109(10): 550–561.
2. Pristera N, Musarra R, Schilz R, et al. The role of echocardiography in the evaluation of pulmonary arterial hypertension. *Echocardiography* 2016; 33(1): 105–116.
3. Bossone E, Bodini BD, Mazza A, et al. Pulmonary arterial hypertension: the key role of echocardiography. *CHEST* 2005; 127(5): 1836–1843.
4. Dell'Italia LJ. Anatomy and physiology of the right ventricle. *Cardiol Clin* 2012; 30(2): 167–187.
5. Grapsa J, Dawson D and Nihoyannopoulos P. Assessment of right ventricular structure and function in pulmonary hypertension. *J Cardiovasc Ultrasound* 2011; 19(3): 115–125.
6. Abduch MC, Assad RS, Mathias WJ, et al. The echocardiography in the cardiovascular laboratory: a guide to research with animals. *Arq Bras Cardiol* 2014; 102(1): 97–103.
7. Gomez-Arroyo JG, Farkas L, Alhussaini AA, et al. The monocrotaline model of pulmonary hypertension in perspective. *Am J Physiol Lung Cell Mol Physiol* 2012; 302(4): L363–369.
8. Haddad F, Hunt SA, Rosenthal DN, et al. Right ventricular function in cardiovascular disease, part I: Anatomy, physiology, aging, and functional assessment of the right ventricle. *Circulation* 2008; 117(11): 1436–1448.
9. de Amorim CR, de Oliveira FB, Barbosa MM, et al. Left ventricular function in patients with pulmonary arterial hypertension: the role of two-dimensional speckle tracking strain. *Echocardiography* 2016; 33(9): 1326–1334.
10. Mauritz GJ, Kind T, Marcus JT, et al. Progressive changes in right ventricular geometric shortening and long-term survival in pulmonary arterial hypertension. *CHEST* 2012; 141(4): 935–943.
11. Joulin O, Marechaux S, Hassoun S, et al. Cardiac force-frequency relationship and frequency-dependent acceleration of relaxation are impaired in LPS-treated rats. *Crit Care* 2009; 13(1): R14.
12. Portnoy SG and Rudski LG. Echocardiographic evaluation of the right ventricle: a 2014 perspective. *Curr Cardiol Rep* 2015; 17(4): 21.
13. Mathai SC, Sibley CT, Forfia PR, et al. Tricuspid annular plane systolic excursion is a robust outcome measure in systemic sclerosis-associated pulmonary arterial hypertension. *J Rheumatol* 2011; 38(11): 2410–2418.
14. Alsoos F and Khaddam A. Echocardiographic evaluation methods for right ventricular function. *J Echocardiogr* 2015; 13(2): 43–51.

15. Haeck ML, Scherptong RW, Marsan NA, et al. Prognostic value of right ventricular longitudinal peak systolic strain in patients with pulmonary hypertension. *Circ Cardiovasc Imaging* 2012; 5(5): 628–636.

16. Puwanant S, Park M, Popovic ZB, et al. Ventricular geometry, strain, and rotational mechanics in pulmonary hypertension. *Circulation* 2010; 121(2): 259–266.

17. Lopez-Candales A. Applicability of automated functional imaging for assessing right ventricular function. *Echocardiography* 2013; 30(8): 919–928.

18. Wright L, Dwyer N, Power J, et al. Right ventricular systolic function responses to acute and chronic pulmonary hypertension: assessment with myocardial deformation. *J Am Soc Echocardiogr* 2016; 29(3): 259–266.

19. Chu M, Gao Y, Zhang Y, et al. The role of speckle tracking echocardiography in assessment of lipopolysaccharide-induced myocardial dysfunction in mice. *J Thorac Dis* 2015; 7(12): 2253–2261.

20. Aguero J, Ishikawa K, Hadri L, et al. Characterization of right ventricular remodeling and failure in a chronic pulmonary hypertension model. *Am J Physiol Heart Circ Physiol* 2014; 307(8): H1204–1215.

21. Alencar AK, Pereira SL, da Silva FE, et al. N-acylhydrazone derivative ameliorates monocrotaline-induced pulmonary hypertension through the modulation of adenosine AA2R activity. *Int J Cardiol* 2014; 173(2): 154–162.

22. Kranias EG and Hajjar RJ. Modulation of cardiac contractility by the phospholamban/SERCA2a regulatome. *Circ Res* 2012; 110(12): 1646–1660.

23. Haghighi K, Bidwell P and Kranias EG. Phospholamban interactome in cardiac contractility and survival: A new vision of an old friend. *J Mol Cell Cardiol* 2014; 77: 160–167.

24. MacLennan DH and Kranias EG. Phospholamban: a crucial regulator of cardiac contractility. *Nat Rev Mol Cell Biol* 2003; 4(7): 566–577.

25. Yin X, Wang L, Qin G, et al. Rats with chronic, stable pulmonary hypertension tolerate low dose sevoflurane inhalation as well as normal rats do. *PLoS ONE* 2016; 11(5): e154154.

26. Qin G, Luo H, Yin X, et al. Effects of sevoflurane on hemodynamics and inducible nitric oxide synthase/soluble guanylate cyclase signaling pathway in a rat model of pulmonary arterial hypertension. *Anesth Analg* 2017; 125(1): 184–189.

27. Roberge S, Roussel J, Andersson DC, et al. TNF-alpha-mediated caspase-8 activation induces ROS production and TRPM2 activation in adult ventricular myocytes. *Cardiovasc Res* 2014; 103(1): 90–99.